N. P. SUH
Associate Professor,
College of Engineering,
University of South Carolina,
Columbia, S. C. Assoc. Mem. ASME

Helical Coils as Impact Load Dispersers

The concept of using tangentially loaded helical coils as impact load dispersers was examined experimentally and theoretically in order to evaluate its effectiveness in minimizing the amplitude of shock loading. It was found that the initial stress pulse decomposed into several pulses of continuously decreasing amplitude as it propagated along the coil. The initial elastic compressive pulse became sinusoidal with frequencies equal to the natural frequencies of the coil shortly after the initial disturbance. It was observed experimentally that there was always a component of the stress pulse which propagated along the helical coil at a velocity close to the bar velocity, $(E/\rho)^{1/2}$. The theoretical analysis showed that there are two modes of wave propagation for the radial flexural and tangential deformation. The group velocity for the tangential deformation modes increases quickly from zero to the bar velocity as the wavelength decreases, especially at a large principal radius of the curvature. The group and the phase velocities for the twist and axial flexural deformation of the coil are also given.

Introduction

Efforts have been made in the past to find effective means of dispersing impact loads so that a high amplitude input stress pulse would degenerate into a wave of low amplitude to minimize the effect of shock loading. The desirability of such a system is obvious. Although different approaches have been tried, none of the attempts have been successful. This paper deals with the use of a helical coil as an impact load disperser.

The concept is illustrated in Fig. 1. An impulse of varying duration is applied tangentially to the helical coil. The coil has straight sections at each end and the impulse is applied at one end. When the stress pulse is incident upon the curved section, the pulse cannot continue along the coil with its original linear pulse if conservation of momentum is to be satisfied. Therefore, it is expected that the shape of the pulse changes as it is partially reflected from the lateral surface.

Another way of explaining what might happen in the coil is to recall that in solids an incident distortional wave can generate dilatational and distortional waves upon reflection. Similarly, an incident dilatational wave may generate distortional and dilatational reflected waves, the angles of reflection of which depend on the incident angle and the material properties of the wave guide. When a distortional wave is incident upon a free boundary, there may not be any dilatational component reflected

Contributed by the Design Engineering Division and presented at the Winter Annual Meeting, Los Angeles, Calif., November 16–20, 1969, of The American Society of Mechanical Engineers. Manuscript received at ASME Headquarters, July 2, 1969. Paper No. 69-WA/DE-3.

Nomenclature

A = cross-sectional area of rod
a = radius of coil projected onto plane perpendicular to its axis
B = function defined in text
C_0 = bar velocity = $(E/\rho)^{1/2}$
C_g = group velocity
C_p = phase velocity
C_s = shear wave velocity = $(G/\rho)^{1/2}$
C = torsional rigidity
c = elevation constant = $h/2\pi$
E = Young's modulus
F = force along axis indicated by subscripts
f = frequency
G = shear modulus
h = distance between adjacent coils
I = moment of inertia of mass per unit length
J = moment of inertia of cross-sectional area
k = wave number for u-w mode
k_1 = wave number for β-v mode
L_1, L_2, L_3 = direction cosines defined by equation (5)
M_1, M_2, M_3 = direction cosines defined by equation (5)
M = bending moment about axis indicated by subscripts
m = mass per unit length
N_1, N_2, N_3 = direction cosines defined by equation (5)
P = arbitrary point on coil
p = angular frequency for u-w mode
p_1 = angular frequency for β-ν mode
R = radius of principal curvature of centroidal axis of cross section

(Continued on next page)

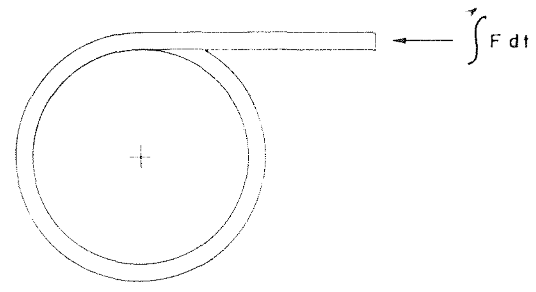

Fig. 1 Part of a helical coil

if the incident angle exceeds a critical value. The geometry of the coil is such that the incident angle to the lateral surface varies continuously along its length. As a consequence, a pulse traveling in the coil is expected to disperse. It should be noted, however, that if a purely twisting moment is applied to the end of the coil, the distortional wave generated in this case is such that it travels down the coil without any dispersion. This is the case with the usual axially loaded helical spring.

The foregoing physical consideration indicates that perhaps a tangentially loaded helical coil may serve as an impact load disperser by lowering the amplitude of the pulse and by increasing the pulse length. It seems that this concept has not been considered by others, although the vibrations of curved rods, including a helical coil, were investigated by Lamb [1],[1] Michell [2], and Love [3]. Philipson [4] extended some of the earlier work by including the extension of the locus of centroids of the cross section of a curved rod. The influence of the thickness of rings on flexural vibration was investigated by Buckens [5].

This paper establishes that for certain applications, helical coils, when tangentially loaded, can disperse stress pulses effectively. The experimental results presented in this paper are new. They are evaluated using the results of an approximate theoretical analysis of stress wave propagation in an infinite coil. The exact mathematical analysis of the experimental results is difficult, but a qualitative understanding of the experimental results can be obtained from the analysis.

Experiments

A helical coil was made of a commercially pure aluminum rod of $^1/_2$-in. dia as shown in Fig. 2. The internal diameter of the coil was 10 in., and the linear length of the coil was 356 in. The coil had about 10 turns and the distance between each coil was about 1 in. The coil had straight ends, at one of which a hammer was dropped from a known height to generate the stress pulses. The length of the straight portion of the coil was made much longer than twice the length of the hammer in order to make certain that the wave reflected from the curved section of the coil would not affect the generation of the pulse at the impact end. In order to prevent plastic deformation at the impact end of the coil a 1.5-in-long spacer made of an aluminum alloy was placed between the hammer and coil. The aluminum alloy had the same mechanical impedance as the commercially pure aluminum. The ends of the coil and the spacer were carefully lapped for complete transmission of the stress pulse across the interface. The other end of the spacer was rounded off in order to insure that the impact occurred at the center of the cross section of the rod for purely axial loading without any bending. The coil was supported near the end opposite from the impact end so that the propagation of the waves was not affected by the supports.

Three different hammer sizes were used to vary the wavelength of the stress pulse. Two of the hammers were made of the same aluminum alloy as the spacer. One of the hammers was $^1/_2$ in. in dia and 6 in. long. The other was 4.5 in. long and $^1/_2$ in. in dia. The third hammer was a $^1/_2$-in-dia steel ball. The pulses generated by the two cylindrical hammers were long enough so that dispersion in the straight section did not exist. Although the pulse generated by the steel ball is expected to disperse in the straight section, the effect may be neglected because of its short length. The cylindrical hammers were mounted on two nylon sliders which slid down a guide from a predetermined height for impact with the coil. The steel ball was dropped through a copper tube, one end of which was placed just above the impact end of the coil. The hammers were dropped from 25 in.

The stress pulses were monitored by using strain gages mounted along the coil. The location of the strain gages and the linear length from the impact end to the gages, measured along the inner radius of the coil, are shown in Fig. 2. At each position, a set of two strain gages (designated by A) were mounted along the axial direction of the bar at 180 deg apart (or the tangential direction of the coil) to measure the axial elongation and another set of strain gages (designated by B) 180 deg apart from each other was mounted to measure the circumferential expansion of the bar. The outputs from the bridge circuits were amplified by solid-state amplifiers, the outputs of which were in turn supplied to an oscilloscope, Tektronix 555. The strain gages used were paper-mount foil gages, BLH FAP-12-12. The beam of the oscilloscope was made to trigger when the hammer came into contact with the coil. The pair of strain gages were connected in series.

Experimental Results

The experimental results are shown in Figs. 3–5. Figs. 3 were obtained with a 6-in-long aluminum hammer. The designations

[1] Numbers in brackets designate References at end of paper.

Nomenclature

s = length of coil
t = time
U, V, W = functions defined in text
u, v, w = displacements along x_1, y_1, and z_1-axes, respectively
x, y, z = coordinate axes defined in text
Z = property of cross section defined in text
β = direction cosine between x_1 and y_0
γ = radius of gyration
δ = defined by equation (3)
ϵ = axial strain defined by equation (6)
κ = radius of curvature projected on y-z plane
κ' = radius of curvature projected on x-z plane
$\bar{\kappa}$ = defined by equation (12)
$\bar{\kappa}'$ = defined by equation (12)
λ = wavelength of sinusoidal wave
ν = Poisson's ratio
ρ = mass density
σ = stress, first subscript designates axis perpendicular to plane and the second subscript designates direction
τ = twist
$\bar{\tau}$ = defined by equation (12)
φ = angle of rotation

Subscripts

0 = unstrained
1 = strained
x = along or about x_1-axis
y = along or about y_1-axis
z = along or about z_1-axis

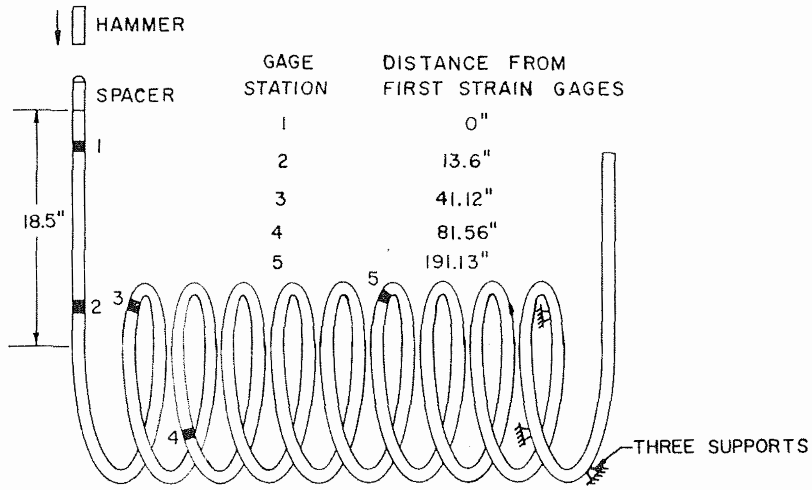

Fig. 2 Experimental arrangement and gage locations

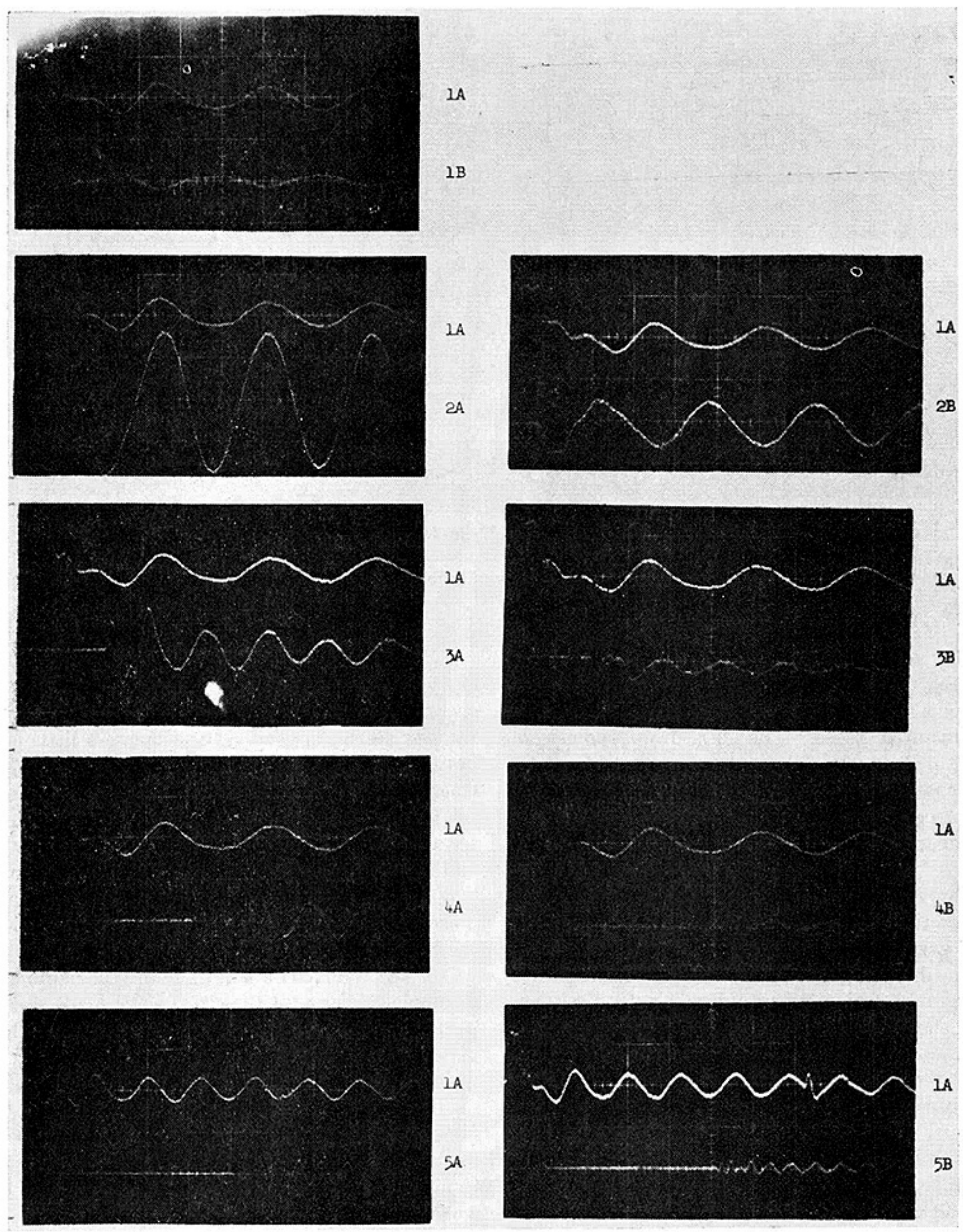

Fig. 3 Experimental results obtained using a 6-in-long hammer. The lower beam was amplified 1.5 times the upper beam. Sweep speed = 1×10^{-4} cm/sec (for all except No. 5). (2×10^{-4} cm/sec for No. 5.)

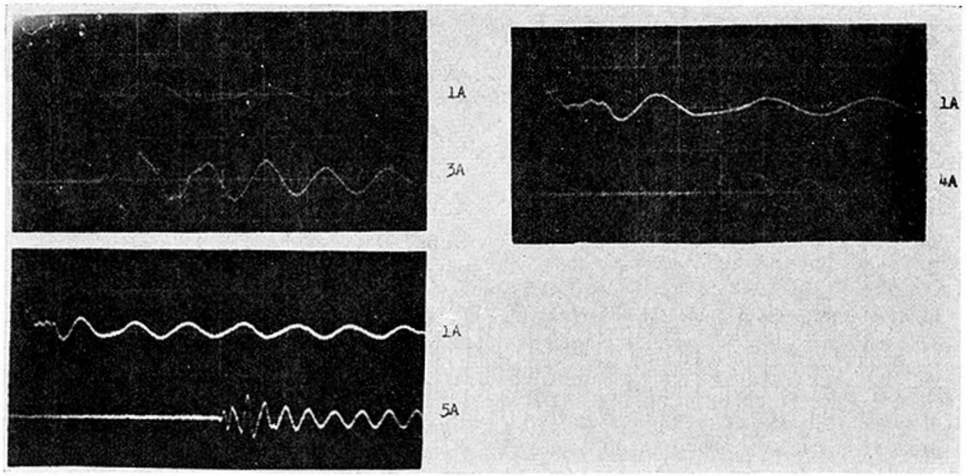

Fig. 4 Experimental results obtained using a $4^1/_2$-in-long hammer—otherwise same as Fig. 3

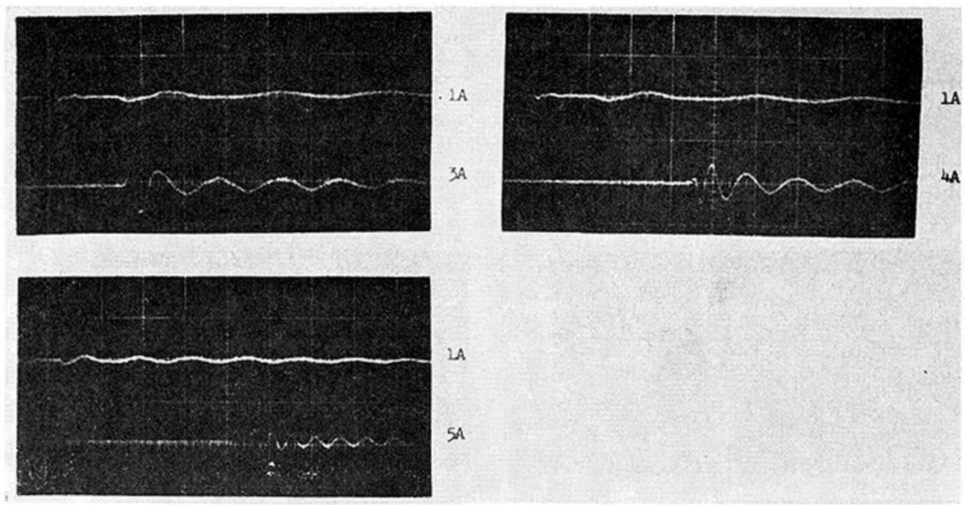

Fig. 5 Experimental results obtained using a $^1/_2$-in-dia steel ball—otherwise same as Fig. 3

are such that the first number denotes the location of the strain gages, as shown in Fig. 2. The second letter indicates the orientation of the gages, A for the axially mounted and B for the circumferentially mounted gages. The data from typical results are tabulated in Table 1. These data were obtained by projecting the pictures taken of the oscilloscope trace on a screen and measuring the necessary information. Efforts were made to be consistent in measurements of the distances between the points.

In Figs. 3–5 the lower beam was amplified 1.5 times the upper beam. In all the pictures, the upper beam trace was obtained from the first set of gages and the lower beams were taken at the stations denoted in the margin. The sweep speed was 10^{-4} sec/cm except at the last station, where it was 2×10^{-4} sec/cm. In these pictures it should be noted that the incident pulse is in general decomposed into many small pulses as it propagates down the coil, as anticipated. The initial pulses are followed by a quasi-steady oscillatory motion of a reasonably constant frequency.

The group velocities are shown in the fourth column in Table 1. They were obtained by dividing the shortest distance the pulse traveled, which is the distance along the inner radius of the coil, by the time taken to reach the particular strain gage station from the first set of strain gages. They indicate that the front of the wave reached all strain gage stations with a velocity close to the bar velocity, which for this aluminum was 1.98×10^5 ips. The accuracy of the measurements is within ± 3 percent. The group velocity seems, in general, to decrease a little as the stress pulse propagates further along the coil, regardless of the initial pulse length, although it remains fairly close to the bar velocity.

The fifth column lists the pulse length of the first pulse in microseconds. The first subcolumn gives the pulse length measured at the first station, while the second subcolumn gives the pulse length as the first pulse reaches the particular gage station. The pulse length at the first station is longer than twice the length of the hammer. This is due to the fact that the impact end of the spacer was rounded off and therefore the hammer did not come to a complete stop until the stress wave made several excursions in it, the hammer continuing to exert pressure on the coil during this period. It should also be noted that the length of the first pulse which is at the front of the degenerated wave becomes shorter and shorter as it travels down the coil.

The sixth column gives the relative amplitudes of the pulses in relation to the incident pulse amplitude. The second number for the upper trace is the amplitude of the sinusoidal portion of the wave measured at the first strain gage station. The numbers for the lower trace give the amplitudes of the succeeding pulses and the amplitude of the oscillatory part. When the quasi-steady

Table 1 Tabulation of experimental results

No.	Lower Trace Strain Gage	Lower Trace Arrival Time (millisec)	Group Vel. (10^{-5} $\frac{in}{sec}$)	Initial Pulse Length (μ sec) Upper	Initial Pulse Length (μ sec) Lower	Relative Amplitudes, Upper Trace 1st.	Relative Amplitudes, Upper Trace Steady	Relative Amplitudes, Lower Trace 1st.	Lower Trace 2nd.	Lower Trace 3rd.	Lower Trace 4th.	Lower Trace Steady	Half Period (millisec.) Upper	Half Period (millisec.) Lower
1	1-B	---	---	133	133	1.0	0.29	0.34	----	----	----	0.09	0.108	0.124
2	1-B	---	---	133	133	1.0	0.29	0.33	----	----	----	0.10	0.110	0.125
3	2-A	0.067	2.029	133	78	1.0	0.29	0.96	----	----	----	0.80	0.104	0.125
4	2-A	0.067	2.029	133	80	1.0	0.30	0.95	----	----	----	0.77	0.107	0.125
5	2-B	0.067	2.029	133	80	1.0	0.28	0.38	----	----	----	0.27	0.107	0.130
6	3-A	0.206	1.996	133	28	1.0	0.28	0.39	0.39	0.50	0.22	0.24	0.106	0.074
7	3-A	0.203	2.026	133	30	1.0	0.30	0.33	0.36	0.47	0.24	0.24	0.103	0.074
8	3-B	0.206	1.996	133	30	1.0	0.28	0.18	0.06	0.22	----	0.07	0.109	0.074
9	4-A	0.405	2.014	133	15	1.0	0.30	0.11	0.28	0.25	0.28	0.21	0.103	0.069
10	4-B	0.412	1.980	133	20	1.0	0.27	0.08	0.08	0.09	0.08	0.06	0.109	0.069
11	5-A	1.015	1.883	133	15	1.0	0.23	0.09	0.18	0.20	0.18	0.15	0.130	0.063
12	5-B	1.00	1.911	133	15	1.0	0.30	0.07	0.25	0.15	0.25	0.06	0.106	0.063
13	1-B	----	----	106	106	1.0	0.23	0.33	----	----	----	0.07	0.106	0.125
14	2-A	0.068	2.000	106	80	1.0	0.24	0.92	----	----	----	0.60	0.103	0.125
15	2-B	0.067	2.029	106	80	1.0	0.23	0.36	----	----	----	0.20	0.089	0.125
16	3-A	0.200	2.056	106	28	1.0	0.23	0.32	0.51	0.35	0.25	0.24	0.098	0.075
17	3-B	0.212	1.940	106	30	1.0	0.23	0.20	0.09	0.20	----	0.09	0.109	0.075
18	4-A	0.417	1.955	106	15	1.0	0.22	0.11	0.31	0.20	0.42	0.17	0.106	0.069
19	4-B	0.417	1.955	106	15	1.0	0.21	0.05	0.09	0.13	0.12	0.08	0.106	0.069
20	5-A	1.030	1.856	106	20	1.0	0.21	0.09	0.18	0.12	0.20	0.14	0.114	0.063
21	5-B	1.00	1.911	106	20	1.0	0.24	0.04	0.07	0.06	0.06	0.06	0.103	0.063
22	1-B	----	----	39	39	1.0	0.14	0.31	----	----	----	0.02	0.103	0.125
23	2-A	0.063	2.159	39	39	1.0	0.11	0.79	----	----	----	0.25	0.092	0.125
24	2-B	0.069	1.971	39	39	1.0	0.14	0.32	----	----	----	0.10	0.097	0.125
25	3-A	0.200	2.056	39	20	1.0	0.15	0.29	0.60	0.24	----	0.16	0.097	0.075
26	3-B	0.206	1.996	39	20	1.0	0.13	0.11	0.13	0.17	----	0.06	0.091	0.075
27	4-A	0.420	1.942	39	10	1.0	0.11	0.09	0.48	0.48	0.42	0.20	0.100	0.069
28	4-B	0.430	1.897	39	10	1.0	0.11	0.07	0.15	0.19	0.10	0.05	0.100	0.069
29	5-A	1.00	1.911	39	10	1.0	0.11	0.05	0.24	0.25	0.33	0.30	0.091	0.063
30	5-B	1.00	1.911	39	10	1.0	0.11	0.07	0.10	0.14	0.10	0.05	0.103	0.063

oscillatory motion follows the first pulse immediately, without any second or third pulses, the space for the succeeding pulses is left blank. It is interesting to note that in all cases the amplitude of the first pulse is lower than those of the next few succeeding pulses. The ratios of the amplitude of the first pulse to those of the succeeding pulses became more pronounced as the distance the pulse travels is greater. The ratios increase more with the longitudinal components than with the circumferential components.

From the relative amplitude measurements given in Table 1, it is seen that in the straight section of the coil the ratio of the 1-B to the 1-A measurements yields the value for Poisson's ratio as 0.33, which is the value one obtains from quasi-static experiments. However, at other positions in the curved part of the coil, the ratio of the circumferential strain to the longitudinal strain becomes much larger than 0.33, indicating the state of stress is not uniaxial and is therefore quite complicated.

The seventh column lists the half periods of the quasi-steady oscillatory components. The periods in the curved section are all nearly the same, being equal to the natural frequency of oscillation as discussed in a later section.

It should be noted that since the strain gages were connected in series, the measurements made by the "A" gages partly cancelled the bending effect, but because of the initial curvature of the rod a small fraction of the bending was measured by the gages. The stress in a curved beam is given by [6]

$$\sigma = \frac{M}{AR}\left(1 + \frac{1}{Z}\frac{y}{R+y}\right), \tag{1}$$

where Z for the circular cross section is

$$Z = -1 + 2\left(\frac{R}{A}\right)^2 - 2\left(\frac{R}{A}\right)\left[\left(\frac{R}{A}\right)^2 - 1\right]^{1/2}.$$

y is measured from the centroidal axis, being positive when measured toward the convex side. Therefore, the stress is not symmetrical about $y = 0$. For the coil under consideration, the stress at the outer radius of the coil is

$$\frac{\sigma A R}{M} = 75.375,$$

while the stress at the inner radius is

$$\frac{\sigma A R}{M} = 81.234.$$

Therefore, it is seen that about 7 percent of the bending stress is not cancelled out. The "B" gages are not influenced by bending.

Theoretical Analysis

The problem to be considered here is the determination of phase velocity, group velocity, and the natural frequency of oscillation of a helical coil in order to investigate the nature of wave propagation in a tangentially loaded helical coil. The coil will be assumed to be infinitely long and an infinite train of sinusoidal waves will be assumed to propagate in the coil. The derivation of the basic equations of motion is given in Love [3] and Philipson [4] and therefore will not be discussed in detail here. The analysis here will disregard any variation across the cross section of the coil and the lateral expansion of the coil.

Basic Relations. Consider a right-handed helical coil whose radius projected onto the plane perpendicular to the axis of the helix is a. It can be readily shown that the principal radius of curvature of the coil lies on planes parallel to this plane, pointing toward the axis of the coil, and is given by

$$R = \frac{a}{\cos^2\delta} = \frac{a^2 + c^2}{a}, \tag{2}$$

where δ is given by

$$\delta = \tan^{-1}(c/a). \tag{3}$$

The principal radius of curvature R may be decomposed into components. For this purpose let us define a moving coordinate system (x_0, y_0, z_0) on the unstrained coil at an arbitrary point P_0. The coordinate system is defined such that z_0 is tangent to the coil at P_0 and x_0 is parallel to the principal normal, n, the positive direction of x_0 being the same as that of n. The y_0-axis is oriented such that the coordinate system makes a right-handed coordinate system. Then, the curvatures projected on the x_0-z_0 plane and the y_0-z_0 plane are, respectively, given by

$$\kappa_0' = 1/R, \qquad \kappa_0 = 0. \tag{4}$$

The configuration of a curved rod can be described completely, if in addition to equations (4), the "twist" τ_0 is given, which is the rate of the change of the binormal along the rod. The binormal vector is perpendicular to the principal normal and tangent vectors in such a way that the tangent, principal, and binormal vectors, in this order, have the right-handed sense.

Now let the coil undergo elastic deformation. The point P_0 on the unconstrained coil will now be at P_1. At P_1 construct a reference frame (x_1, y_1, z_1) such that z_1 is tangent to the coil at P_1 of the strained coil. x_1 is defined such that the x_1 and z_1-axes lie on the plane which is tangent at P_1 to the strained rod material originally in the (x_0, z_0) plane. y_1 is again chosen such that the (x_1, y_1, z_1) coordinate system is a right-handed one. After deformation, the original increment of length Δs_0 becomes Δs_1. The coordinate system (x_0, y_0, z_0) is related to the (x_1, y_1, z_1) system by direction cosines as

	x_0	y_0	z_0
x_1	L_1	M_1	N_1
y_1	L_2	M_2	N_2
z_1	L_3	M_3	N_3.

(5)

L_1, L_2, L_3, M_1, etc., are direction cosines between the axes indicated. The elongation of the fiber through the centroids may be expressed as

$$\frac{ds_1}{ds_0} = 1 + \epsilon. \tag{6}$$

The direction cosines are found to be, to the first order,

$$\begin{aligned} L_3 &= \frac{\partial u}{\partial s_0} + \frac{w}{R} \\ M_3 &= \frac{\partial v}{\partial s_0} \\ N_3 &= 1 \\ L_1 &= M_2 = 1 \\ M_1 &= -L_2 = \beta \\ N_1 &= -L_3 \\ N_2 &= -M_3. \end{aligned} \tag{7}$$

The axial strain may be written as

$$\epsilon = \frac{\partial w}{\partial s_0} - \frac{u}{R}. \tag{8}$$

The equations of motion can be written as

$$\begin{aligned} &\frac{\partial F_x}{\partial s_0} - \bar{\tau}_1 F_y + \bar{\kappa}_1' F_z = m(1+\epsilon)\frac{\partial^2 u}{\partial t^2} \quad \text{along the } x_1\text{-axis} \\ &\frac{\partial F_y}{\partial s_0} - \bar{\kappa}_1 F_z + \bar{\tau}_1 F_x = m(1+\epsilon)\frac{\partial^2 v}{\partial t^2} \quad \text{along the } y_1\text{-axis} \\ &\frac{\partial F_z}{\partial s_0} - \bar{\kappa}_1' F_x + \bar{\kappa}_1 F_y = m(1+\epsilon)\frac{\partial^2 w}{\partial t^2} \quad \text{along the } z_1\text{-axis} \\ &\frac{\partial M_x}{\partial s_0} - \bar{\tau}_1 M_y + \bar{\kappa}_1' M_z - F_y(1+\epsilon) = I_x(1+\epsilon)\frac{\partial^2 \varphi_x}{\partial t^2} \\ &\qquad \text{rotation about the } x_1\text{-axis} \\ &\frac{\partial M_y}{\partial s_0} - \bar{\kappa}_1 M_z + \bar{\tau}_1 M_x + F_x(1+\epsilon) = I_y(1+\epsilon)\frac{\partial^2 \varphi_y}{\partial t^2} \\ &\qquad \text{rotation about the } y_1\text{-axis} \\ &\frac{\partial M_z}{\partial s_0} - \bar{\kappa}_1' M_x + \bar{\kappa}_1 M_y = I_z(1+\epsilon)\frac{\partial^2 \varphi_z}{\partial t^2} \\ &\qquad \text{rotation about the } z_1\text{-axis,} \end{aligned} \tag{9}$$

where the forces acting on the cross section at P_1 are defined by

$$\begin{aligned} F_x &= \int \sigma_{zx} dA \\ F_y &= \int \sigma_{zy} dA \\ F_z &= \int \sigma_{zz} dA, \end{aligned} \tag{10}$$

and the couples are defined by

$$\begin{aligned} M_x &= \int y_1 \sigma_{zz} dA \\ M_y &= \int x_1 \sigma_{zz} dA \\ M_z &= \int (x_1 \sigma_{zy} - y_1 \sigma_{zx}) dA. \end{aligned} \tag{11}$$

It should be noted that these couples and forces are written with respect to the (x_1, y_1, z_1)-axes, but for small deformations the x_1, y_1, and z_1-directions almost coincide with x_0, y_0, and z_0, respectively. $\bar{\kappa}_1$, $\bar{\kappa}_1'$, and $\bar{\tau}_1$ are related to the components of the principal curvature of the strained rod at P_1, i.e., κ_1, κ_1', and τ_1, by

$$\begin{aligned} \bar{\kappa}_1 &= \kappa_1(1+\epsilon) \\ \bar{\kappa}_1' &= \kappa_1'(1+\epsilon) \\ \bar{\tau}_1 &= \tau_1(1+\epsilon), \end{aligned} \tag{12}$$

where

$$\begin{aligned} \bar{\kappa}_1 &= \frac{\beta}{R} - \frac{\partial^2 v}{\partial s_0^2} \\ \bar{\kappa}_1' &= \frac{1}{R} + \frac{\partial^2 u}{\partial s_0^2} + \frac{1}{R}\frac{\partial w}{\partial s_0} \\ \bar{\tau}_1 &= \frac{\partial \beta}{\partial s_0} + \frac{1}{R}\left(\frac{\partial v}{\partial s_0}\right). \end{aligned} \tag{13}$$

The moments and the axial force given in equations (10) and (11) may be related to the curvature and strain as

$$\begin{aligned} M_x &= EJ_x(1-\epsilon)\left(\frac{\beta}{R} - \frac{\partial^2 v}{\partial s_0^2}\right) \\ M_y &= EJ_y\left(\frac{u}{R^2} + \frac{\partial^2 u}{\partial s_0^2}\right) \\ M_z &= C\left(\frac{\partial \beta}{ds_0} + \frac{1}{R}\frac{\partial v}{\partial s_0}\right) \\ F_z &= EA\left(\frac{\partial w}{\partial s_0} - \frac{u}{R}\right), \end{aligned} \tag{14}$$

where J_x and J_y are the moments of inertia of the cross section about the x_1 and y_1-axis, respectively. The angles of rotation about the x_1, y_1, and z_1-axes are, respectively

$$\begin{aligned} \varphi_x &= -\frac{\partial v}{\partial s_0} \\ \varphi_y &= \frac{\partial u}{\partial s_0} + \frac{w}{R} \\ \varphi_z &= \beta. \end{aligned} \tag{15}$$

Substituting equations (12)–(15) into equations (9) and neglecting the higher-order terms, the equations of motion may be written as

$$\frac{\partial F_x}{\partial s_0} + \frac{EA}{R}\left(\frac{\partial w}{\partial s_0} - \frac{u}{R}\right) = m\frac{\partial^2 u}{\partial t^2} \quad \text{along the } x_1\text{-axis}$$

((16a) Continued next page)

$$EA\left(\frac{\partial^2 w}{\partial s_0{}^2} - \frac{1}{R}\frac{\partial u}{\partial s_0}\right) - \frac{1}{R}F_x = m\frac{\partial^2 w}{\partial t^2} \quad \text{along the } z_1\text{-axis} \qquad (16a)$$

$$EJ_y\left(\frac{1}{R^2}\frac{\partial u}{\partial s_0} + \frac{\partial^3 u}{\partial s_0{}^3}\right) + F_x = I_y\frac{\partial^2}{\partial t^2}\left(\frac{\partial u}{\partial s_0} + \frac{w}{R}\right)$$

rotation about the y_1-axis

and

$$\frac{\partial F_y}{\partial s_0} = m\frac{\partial^2 v}{\partial t^2} \quad \text{along the } y_1\text{-axis}$$

$$EJ_x\left(\frac{1}{R}\frac{\partial \beta}{\partial s_0} - \frac{\partial^3 v}{\partial s_0{}^3}\right) - F_y = I_x\frac{\partial^2}{\partial t^2}\left(-\frac{\partial v}{\partial s_0}\right)$$

rotation about the x_1-axis (16b)

$$C\left(\frac{\partial^2 \beta}{\partial s_0{}^2} + \frac{1}{R}\frac{\partial^2 v}{\partial s_0{}^2}\right) = I_z\frac{\partial^2 \beta}{\partial t^2} \quad \text{rotation about the } z_1\text{-axis.}$$

It should be noted that equations (16a) consist of only u, w, and F_x, whereas equations (16b) are functions of only β, v, and F_y. Equations (16a) represent the motion associated with radially flexural deformation. Equations (16b) are related to the twisting and deflection along the y_1-axis which will be zero for purely tangential loading. To the first order, the u-w displacements are not coupled to the β-v deformation, and therefore they may be treated separately.

The u-w Displacement Models. Eliminating F_x from the first and second equations of equation (16a), equations (16a) may be written as

$$\frac{\gamma^2}{C_0{}^2}\frac{\partial^2}{\partial t^2}\left(\frac{\partial^2 u}{\partial s_0{}^2} + \frac{1}{R}\frac{\partial w}{\partial s_0}\right) - \gamma^2\left(\frac{1}{R^2}\frac{\partial^2 u}{\partial s_0{}^2} + \frac{\partial^4 u}{\partial s_0{}^4}\right) + \left(\frac{1}{R}\frac{\partial w}{\partial s_0} - \frac{u}{R^2}\right) = \frac{1}{C_0{}^2}\frac{\partial^2 u}{\partial t^2} \qquad (17)$$

$$\frac{\partial^2 w}{\partial s_0{}^2} - \frac{1}{R}\frac{\partial u}{\partial s_1} - \frac{\gamma^2}{C_0{}^2}\frac{\partial^2}{\partial t^2}\left(\frac{1}{R}\frac{\partial u}{\partial s_0} + \frac{w}{R^2}\right) + \gamma^2\left(\frac{1}{R^3}\frac{\partial u}{\partial s_0} + \frac{1}{R}\frac{\partial^3 u}{\partial s_0{}^3}\right) = \frac{1}{C_0{}^2}\frac{\partial^2 w}{\partial t^2},$$

where

$$I_y = m\gamma^2, \qquad J_y = A\gamma^2,$$

$$\frac{EA}{m} = C_0{}^2.$$

C_0 is the bar velocity.

Assume the solution to equations (16) to be

$$u = U(x_0,y_0)\exp\left[i(kz_0 + pt)\right]$$
$$w = W(x_0,y_0)\exp\left[i(kz_0 + pt)\right], \qquad (18)$$

where

$$p = 2\pi f,$$

$$k = \frac{2\pi}{\lambda}.$$

Note that $z_0 = s_0$ and the phase velocity C_p is given by p/k. Substituting equations (18) into equations (17), the frequency equation is

$$\frac{1}{C_0{}^4}\left(1 + \frac{1}{k^2\gamma^2} + \frac{1}{k^2R^2}\right)p^4 + \frac{1}{C_0{}^2}\left[-\left(2k^2 + \frac{1}{\gamma^2} - \frac{1}{R^2}\right) - \frac{1}{R^2}\left(\frac{1}{k^2\gamma^2} + \frac{1}{k^2R^2} - 2\right)\right]p^2 + \frac{1}{R^4}(1 - k^2R^2)^2 = 0. \qquad (19)$$

It is interesting to note that when $\lambda \to \infty$, $k \to 0$, and

$$p = \left(\frac{EA}{mR^2}\right)^{1/2} = \frac{C_0}{R}. \qquad (20)$$

Equation (20) is the fundamental frequency of the radial mode of vibration.

The phase velocity as obtained from equation (19) is

$$\left(1 + \frac{1}{k^2\gamma^2} + \frac{1}{k^2R^2}\right)\left(\frac{C_p}{C_0}\right)^4 - \left[\left(2 + \frac{1}{k^2\gamma^2} - \frac{3}{k^2R^2}\right) + \frac{1}{k^2R^2}\left(\frac{1}{k^2\gamma^2} + \frac{1}{k^2R^2}\right)\right] \times \left(\frac{C_p}{C_0}\right)^2 + \frac{1}{k^4R^4} \times (1 - k^2R^2)^2 = 0. \qquad (21)$$

For an infinite train of waves the phase velocity gives the difference in phase of the vibration of the helical coil. In a dispersive medium the energy is transmitted at the group velocity which is given by

$$C_g = \frac{dp}{dk}. \qquad (22)$$

Equation (19) yields

$$\frac{C_g}{C_0} = -\frac{B}{D}, \qquad (23)$$

where

$$D = \left(\frac{C_p}{C_0}\right)^3\left[4k^3\left(k^2 + \frac{1}{\gamma^2} + \frac{1}{R^2}\right)\right] + 2\left(\frac{C_p}{C_0}\right)\left[-k^3\left(k^2 + \frac{1}{\gamma^2}\right) + \frac{k^3}{R^2}\left(3 - k^2R^2 - \frac{1}{k^2\gamma^2} - \frac{1}{k^2R^2}\right)\right]$$

$$B = 2k^5\left(\frac{C_p}{C_0}\right)^4 + \left(\frac{C_p}{C_0}\right)^2\left[-4k^5 - \frac{2k^3}{\gamma^2} + \frac{2k^3}{R^2}(3 - 2k^2R^2)\right] + \frac{2k}{R^4}(1 - k^2R^2)(1 - 3k^2R^2).$$

Equation (21) may have two real, positive roots, corresponding to two different modes of wave propagation. The roots for C_p are shown in Figs. 6 and 7. The corresponding group velocities are shown in Figs. 8 and 9. As the wavelength approaches infinity, C_p approaches either infinity or a minimum value at $k = 1/R$ and then increases again. The group velocity of the first mode approaches zero as the wavelength approaches infinity; whereas the group velocity of the second mode approaches a minimum value at $k = 1/R$. With further decrease in k, the group velocity of the second mode assumes negative values, signifying that the second mode does not propagate for $k < 1/R$. When k becomes very small, the group velocity again becomes positive, but it does not have any physical significance. On the other hand, as the wavelength becomes smaller, both of these phase velocities and the group velocities approach the bar velocity C_0. If the wavelength becomes too small, i.e., approximately $\lambda < (5.6\pi\gamma^2)/R$, the roots for the phase velocity become complex, the complex part being three to four orders of magnitude smaller than the real part. The complex part probably does not exist in a more exact analysis.

Each mode will be discussed separately. The group velocity of the first mode of the u-w deformation rapidly approaches the bar velocity as k increases from zero, especially at large values of the principal radius of curvature. In the limit, as the radius of curvature approaches infinity (i.e., straight bar), the group and the phase velocities are equal to the bar velocity. It should be noted that the first mode shown is not affected appreciably by the change in the radius of gyration, except at small radius of curvature as shown by the dotted line of Fig. 8 for $R = 2$. This indicates that the first mode of the u-w deformation is associated with the extensional deformation of the locus of the centroids of the coil cross section.

The second mode of the u-w deformation has small phase and group velocities at large wavelengths compared to those of the first mode. The second mode is nearly independent of the principal radius of curvature, but very much dependent upon the radius of gyration. This second mode is associated with the radially flexible deformation of the coil. The group velocities exceed the bar velocity in a certain range of wavelengths. These curves closely resemble the phase and group velocities predicted by the approximate theory of Rayleigh [7] for the flexural wave propagation in a straight rod. According to the exact theory for a straight rod, the phase and group velocities approach the Rayleigh surface wave velocity rather than the bar velocity predicted by this analysis and by the Rayleigh theory [8]. If the results shown in Figs. 6–9 for the second mode are replotted by replotting the group and phase velocities as a function of a/λ, the resulting curves are nearly the same as those predicted by the Rayleigh theory.

The propagation velocities for the β-v deformation modes are discussed in the Appendix, since they are not directly related to the experimental results.

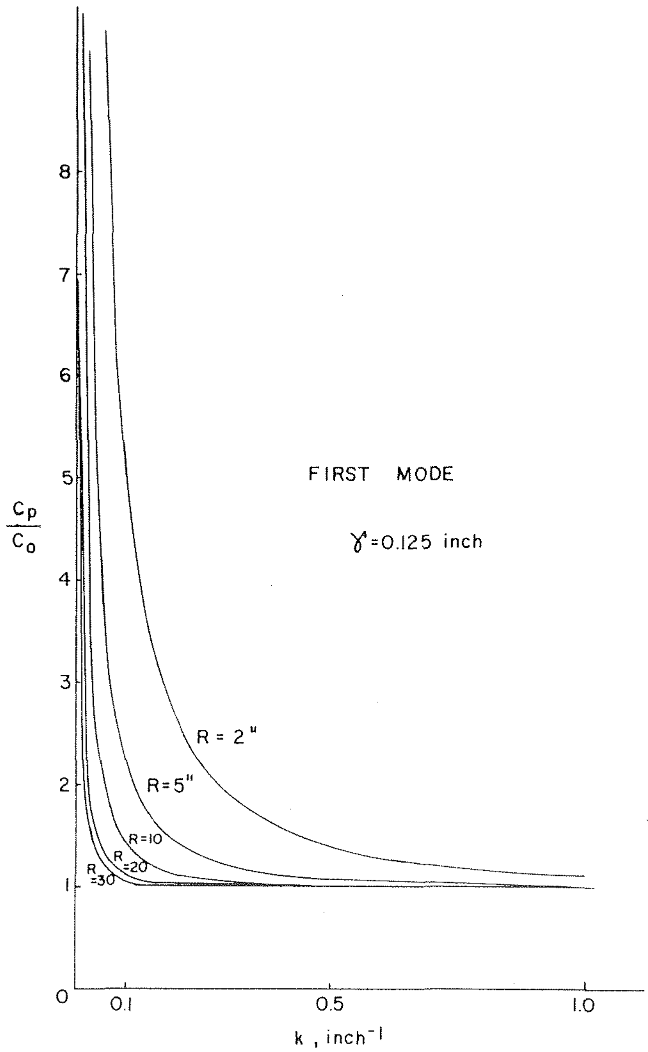

Fig. 6 Phase velocity versus wave number for u-w deformation—first mode

Discussion of Experimental and Theoretical Results

The first mode shown in Figs. 6–9 is associated with the extension of the coil, as stated earlier. Therefore, the stress pulses shown in Figs. 3, 4, and 5 are governed by the group velocity shown in Fig. 8. It is interesting to note that the reason the initial pulse length becomes shorter and shorter is because only the short wavelength components propagate with the bar velocity and the longer wavelength components lag behind. It should be noted that the initial pulse is composed of many waves of various frequencies. Since the high-frequency Fourier components of the pulse have lower amplitudes than the longer wavelength components, the amplitude of the pulse at the front decreases as the pulse propagates along the coil. Consequently, the slower-moving succeeding pulses have higher amplitudes. Also, the length of the pulse that arrives at a given station in the coil first becomes shorter and shorter since it represents the superposition of several short wavelength components.

The experimentally observed decrease in the group velocity

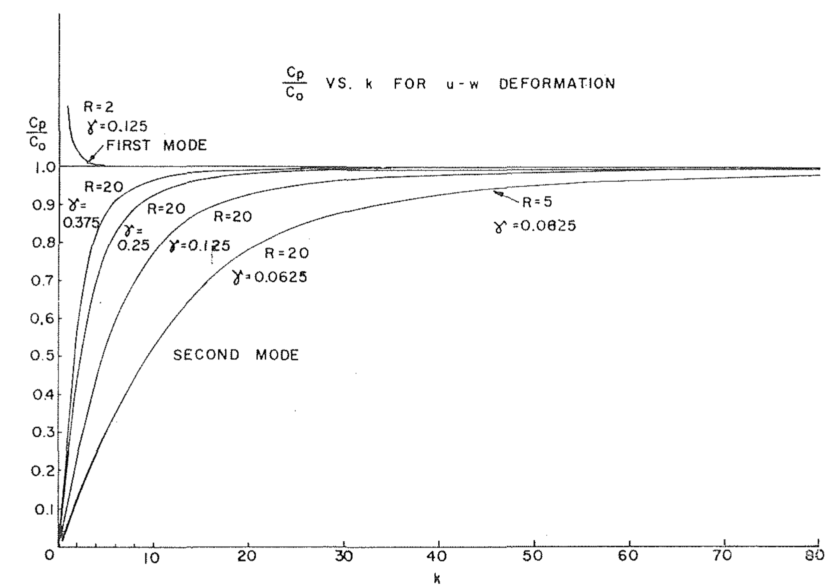

Fig. 7 Phase velocity versus wave number for the u-w deformation—second mode

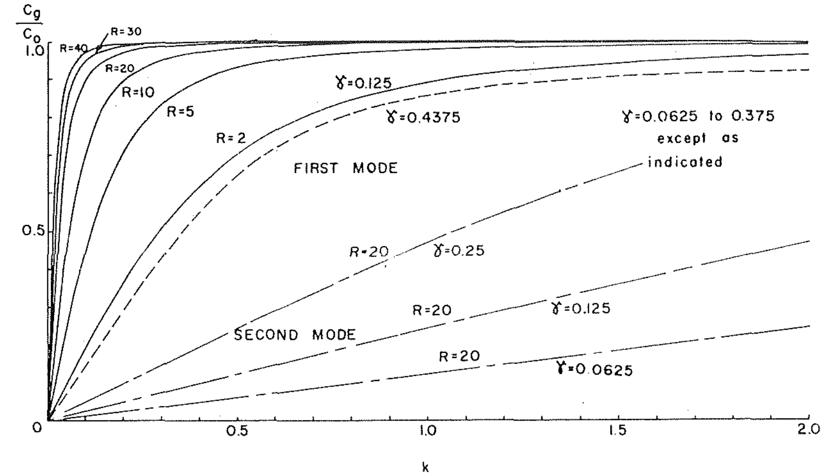

Fig. 8 Group velocity versus wave number for *u-w* deformation—first mode

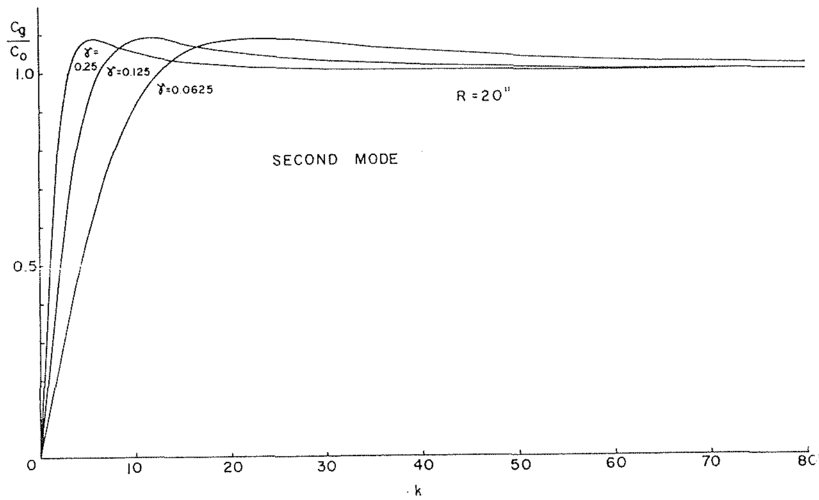

Fig. 9 Group velocity versus wave number for *u-w* deformation—second mode

along the coil may be due to the fact that the short wavelength components which travel at the bar velocity must decrease in amplitude as the pulse disperses continuously. Therefore, the very front of the pulse may have such a low amplitude that it is not measurable. This is substantiated by the decrease in the pulse length as the distance of wave propagation increases. It should be noted that the absolute value of the group velocity calculated from the experimental results may be erroneous since the distance the wave propagated was measured along the shortest path.

The dispersion of the pulse is expected to be greater as the principal radius of curvature decreases, because the difference in the group velocity becomes greater as the radius decreases. It also implies that if the coil is so made that its principal radius of curvature changes continuously, the coil can decompose the initial pulse in an arbitrary manner by controlling the group velocity.

The analysis given in the preceding section states that the natural frequency varies continuously as a function of wavelength. The experimentally measured period decreases, but not in exact accordance with the theoretical predictions, indicating that the simple theory is not sufficient to predict all the experimental results. However, the quasi-steady oscillatory parts have natural frequencies corresponding to the basic mode given by equation (20). The experimental values compare very favorably with the theoretical result of the half period of 0.064×10^{-3} sec.

The experimental results show that the stress is highest in the straight section, when the first incident pulse passes through it. Therefore, the maximum mangitude of the impact stress that may be applied to the coil is limited by the uniaxial dynamic yield stress of the metal, unless a certain amount of plastic deformation can be tolerated. For extremely large loads, this type of impact load disperser may be combined with other shock absorbers in order to extend its usefulness. It may be of interest to note that the adjacent coils never touch each other laterally during the loading.

The duration of loading considered in this paper is relatively short. Additional work is being done to investigate the case of extremely long pulses with high energy. The effects of varying the curvature and pitch have been investigated, the results of which state that for the coil used in this experiment a small variation in the pitch of the coil does not significantly affect the results [9].

Conclusion

A stress pulse in a tangentially loaded helical coil disperses as it propagates along the coil, and the coil may be used as an impact load disperser. The wave-propagation velocity is a function of wavelength, material properties, and the geometry of the coil. The information provided in this paper may be used in designing an impact load disperser.

References

1 Lamb, H., "On the Flexure and the Vibration of a Curved Bar," *London Mathematical Society Proceedings*, Vol. 19, 1888, p. 365.
2 Michell, J. H., "On the Stability of a Bent and Twisted Wire," *Messenger of Mathematics*, Vol. 19, 1890.
3 Love, A. E. H., "The Propagation of Waves of Elastic Displacement Along a Helical Coil," *Cambridge Philosophical Society Transactions*, Vol. 18, 1900.
4 Philipson, L. L., "On the Role of Extension in the Flexural Vibrations of Rings," *Journal of Applied Mechanics*, Vol. 23, Trans. ASME, Vol. 78, 1956, p. 364.
5 Buckens, F., "Influence of the Relative Radial Thickness of a Ring on Its Natural Frequencies," *Journal of the Acoustical Society of America*, Vol. 22, 1950, p. 437.
6 Seely, F. S., and Smith, J. O., *Advanced Mechanics of Materials*, Wiley, New York, 2nd ed., 1952.
7 Lord Rayleigh, *Theory of Sound*, Macmillan, London, 1894.
8 Davies, R. M., "A Critical Study of the Hopkinson Pressure Bar," *Philosophical Transactions*, Series A, Vol. 240, 1948, p. 375.
9 Suh, N. P., "Elastic Wave Propagation in a Helical Coil With Varying Curvature," submitted for publication, 1969.

APPENDIX

The β-v Deformation

The β-v deformation may be neglected in evaluating the experimental results presented in this paper since the loading was purely tangential. However, the analytical results are of interest.

The shear force term F_y may be eliminated from the first and the second equations of equations (16*b*) and the resulting equations may be written as

$$\begin{aligned} \frac{1}{R}\frac{\partial^2\beta}{\partial s_0^2} &= \frac{1}{C_0^2\gamma^2}\left(\frac{\partial^2 v}{\partial t^2}\right) + \frac{1}{C_0^2}\frac{\partial^2}{\partial t^2}\left(\frac{\partial^2 v}{\partial s_0^2}\right) + \frac{\partial^4 y}{\partial s_0^4} \\ \frac{\partial^2\beta}{\partial s_0^2} - \frac{1}{C_s^2}\frac{\partial^2\beta}{\partial t^2} &= -\frac{1}{R}\frac{\partial^2 v}{\partial s_0^2}, \end{aligned} \tag{24}$$

where $C_s^2 = GA/m$.

The solutions for β and v may be assumed to be

$$\begin{aligned} \beta &= B(x_0, y_0)\exp\left[i(k_1z_0 + p_1t)\right] \\ v &= V(x_0, y_0)\exp\left[i(k_1z_0 + p_1t)\right]. \end{aligned} \tag{25}$$

Substituting equations (25) into equations (24), the frequency equation becomes

$$p_1^4\left[\frac{1}{C_s^2C_0^2}\left(\frac{1}{k_1^2\gamma^2}+1\right)\right] - p_1^2\left[\frac{k_1^2}{C_0^2}\left(\frac{1}{k_1^2\gamma^2}+1\right)+\frac{k_1^2}{C_s^2}\right] + k^4\left(1-\frac{1}{R^2k_1^2}\right) = 0 \tag{26}$$

The phase velocity is given by

$$\left(\frac{C_p}{C_0}\right)^4\left[\left(\frac{C_0}{C_s}\right)^2\left(\frac{1}{\gamma^2k_1^2}+1\right)\right] - \left(\frac{C_p}{C_0}\right)^2\left[\left(\frac{1}{k_1^2\gamma^2}+1\right)+\left(\frac{C_0}{C_s}\right)^2\right] + \left(1-\frac{1}{R^2k_1^2}\right) = 0. \tag{27}$$

The group velocity is given by

$$\left(\frac{C_g}{C_0}\right)\left[2\left(\frac{C_p}{C_0}\right)^3\left(\frac{C_0}{C_s}\right)^2\left(\frac{1}{\gamma^2k_1^2}+1\right) - \left(\frac{C_p}{C_0}\right)\left(\frac{1}{k_1^2\gamma^2}+1+\frac{C_0^2}{C_s^2}\right)\right] - \frac{1}{\gamma^2k_1^2}\left(\frac{C_0}{C_s}\right)^2\left(\frac{C_p}{C_0}\right)^4 - \left(\frac{C_p}{C_0}\right)^2\left[1+\left(\frac{C_0}{C_s}\right)^2\right] + \left(2-\frac{1}{k_1^2R^2}\right) = 0. \tag{28}$$

The shear velocity C_s and the bar velocity C_0 are related by

$$\left(\frac{C_0}{C_s}\right)^2 = 2(1+\nu). \tag{29}$$

Equation (27) may have more than one positive, real root, but it is much more complicated than the corresponding equation for the u-w mode. If $k_1 < 1/R$, there is only one real, positive root. If $k_1 > 1/R$, there are two positive, real roots, approaching either the shear wave velocity or the bar velocity. In the limit as k_1 approaches infinity, the group velocity approaches the shear or bar velocity. At $k_1 = 1/R$, C_p may be either equal to zero or

$$\frac{C_p}{C_0} = \left[\left(\frac{C_s}{C_0}\right)^2 + \frac{k_1^2\gamma^2}{1+k_1^2\gamma^2}\right]^{1/2} \tag{30}$$

However, the former value, i.e., $C_p = 0$, is not a physically acceptable solution as the group velocity associated with this phase velocity becomes infinite.

The results are shown in Figs. 10 and 11. It is interesting to

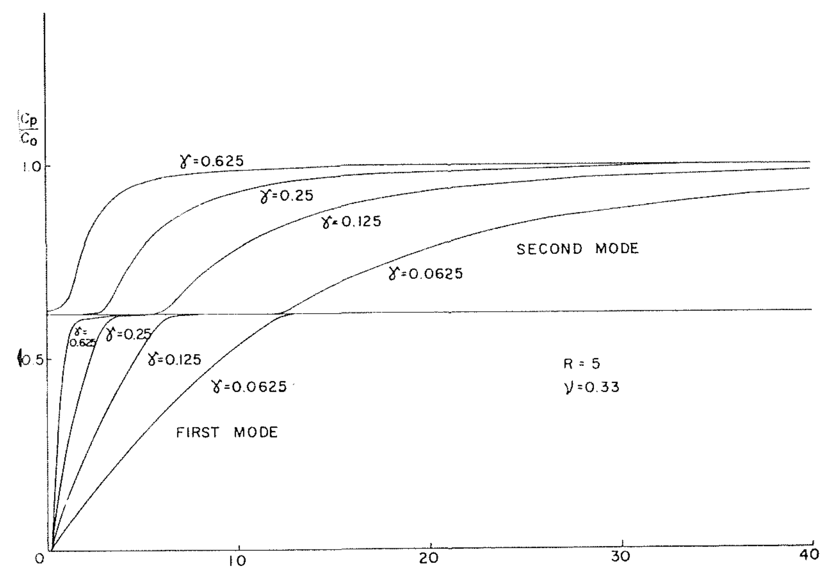

Fig. 10 Phase velocity versus wave number for the β-v deformation

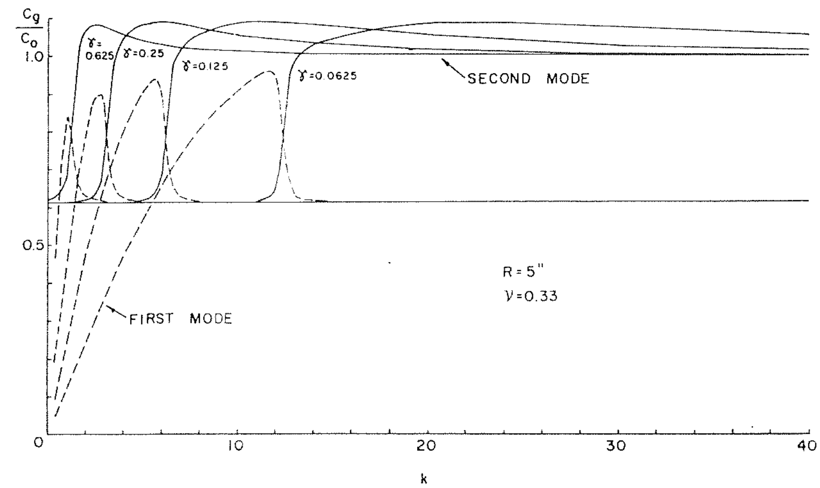

Fig. 11 Group velocity versus wave number for the β-v deformation

note that the combination of the first mode and the second mode nearly always yields phase and group velocities equal to the shear wave velocity C_s. Since a pure twisting wave propagates with the shear wave velocity, it must be that the flexural mode propagates with velocities ranging between zero and the bar velocity, whereas the β deformation propagates with the shear wave velocity, if $k_1 > 1/R$. If $k_1 < 1/R$, the disturbance propagates with velocities close to the shear wave velocity. This is physically reasonable since such a long period of loading results in twisting. The principle of radius of curvature has little influence on the curves shown, but Poisson's ratio does affect the results. Again, the group velocity overshoots the bar velocity in a certain wavelength range which was discussed earlier in connection with the Rayleigh theory for flexural wave propagation in a straight rod.